# Title: Distinct brain networks coupled with the parietal cortex represent target location inside and outside the visual field

**Abbreviated title:** Brain networks represent target locations in visual field

**Authors:** Bo Zhang [1], Fan Wang [5,6,7], Naya Yuji [1, 2, 3, 4, *]

**Affiliations:**

[1] School of Psychological and Cognitive Sciences, Peking University, No. 52, Haidian Road, Haidian District, Beijing 100805, China

[2] IDG/McGovern Institute for Brain Research at Peking University, No. 52, Haidian Road, Haidian District, Beijing 100805, China

[3] Center for Life Sciences, Peking University, No. 52, Haidian Road, Haidian District, Beijing 100805, China

[4] Beijing Key Laboratory of Behavior and Mental Health, Peking University, No. 52, Haidian Road, Haidian District, Beijing 100805, China

[5] State Key Laboratory of Brain and Cognitive Science, Institute of Biophysics, Chinese Academy of Sciences, 15 Datun Road, Beijing 100101, China

[6] CAS Center for Excellence in Brain Science and Intelligence Technology

[7] University of Chinese Academy of Sciences, 19A Yuquan Road, Beijing 100049, China

**Corresponding author:** Yuji Naya

Address: School of Psychological and Cognitive Sciences, Peking University, No. 52, Haidian Road, Wang Kezhen Building, Room 1707,Haidian District, Beijing 100805, China

E-mail: yujin@pku.edu.cn

**Conflict of interest statement**: no competing financial interests

**Acknowledgments:** This work was supported by the National Natural Science Foundation of China Grant 31421003 (to Y.N.). We thank the National Center for Protein Sciences at Peking University for assistance with MRI data collection, and the State Key Laboratory of Brain and Cognitive Science at Chinese Academy of Sciences for assistance with MEG scanning, which was supported in part by the Ministry of Science and Technology of China grant (2019YFA0707103), the National Nature Science Foundation of China grant (31730039), and the Strategic Priority Research Program of Chinese Academy of Science (XDB32010300). Computational work was supported by resources provided by the High-performance Computing Platform of Peking University.

## Abstract

Our mental representation of the egocentric space is influenced by the disproportionate sensory perception along the ventral-dorsal (i.e., front-back) axis of the body. Previous studies typically investigated the neural architectures involved in the egocentric representations within the visual field and revealed a crucial involvement of the parietal cortex and its interaction with the frontal lobe. However, neural architectures involved in the space representation behind self-body are still unclear. To address this problem, we applied both functional magnetic resonance imaging (fMRI) and magnetoencephalography (MEG) to a 3D spatial-memory paradigm for human participants, in which the participants remembered a target location within (left or right) or outside (back) their visual field. Both fMRI and MEG experiments showed that the involvements of the fronto-parietal network including the frontal eye field and supplementary motor area were larger in the representations of retrieved target object within the visual field than outside. Conversely, the medial temporal lobe (MTL)-parietal network, including the right entorhinal cortex, was more involved in the target representation when the target was outside the visual field in both the experiments. In the MEG experiment, the connectivity increased in alpha-band frequency (8–13 Hz) in both fronto-parietal and MTL-parietal networks, and the preferential enhancement of the MTL-parietal network for the back preceded that of the fronto-parietal network for left/right. These findings suggest that the parietal cortex may represent whole space around self-body by coordinating the two distinct brain networks to process the egocentric spatial representation inside and outside the visual field.


**Significance Statement (120 words maximum)**

Representations of external space around self-body are necessary for coordinated actions, and our sensory-motor system is strongly biased toward processing the space in front. However,

space exists behind us too. We conducted both fMRI and MEG studies and found that the parietal cortex coupled with the frontal lobe (FEF and SMA) and medial temporal lobe (MTL) represents a target inside and outside the visual field, respectively, although the target location was retrieved from short-term memory in both conditions. These results suggest that the parietal cortex may represent the whole of the present external space by interacting (alpha rhythm) with the frontal lobe for subsequent actions and the MTL to inquire the back scene.

Key words: egocentric direction, fMRI, MEG, parietal cortex, entorhinal cortex

## Introduction

When we plan to reach for a target, it is necessary to attain its location information in the body-centered reference frame or the so-called "egocentric" spatial coordinate (Stein, 1989; Shelton and McNamara, 1997; Burgess, 2006). Previous studies using humans and nonhuman primates as subjects indicated crucial involvements of the parietal cortex in the representations of egocentric location for sensory perception, motor action, and their coordination (Khan, 2008; Ciaramelli et al., 2010; Iriki and Taoka, 2012; Wang et al., 2016; Zhou et al., 2018). Anatomically, the parietal cortex is located at the final stage of the dorsal pathway, which is often named either "where" or "how" pathway (Goodale and Milner 1992; Ungerleider et al., 2008). Perceptual signals including visual and somatosensory information thus converge on the parietal cortex, which interacts with the frontal eye field (FEF)—the region associated with attention and eye movement toward a target in the external space around the self (Stein, 1992; Desmurget et al., 1999; Donner, 2000). These anatomical connection patterns are consistent with those reported by neuropsychological studies, i.e., a damaged parietal cortex shows impaired egocentric spatial awareness known as hemispherical neglect, which leads to neglect of a target on one side of a field of vision (Vallar, 1998). Hemispherical neglect appears not only in perception but also in the memory field, known as "representational neglect" (Bisiach and Luzzatti, 1978). With accumulating human imaging studies examining spatial navigation and episodic recollection (Farrer and Frith, 2002; Spiers and Maguire, 2007; Gaesser et al., 2013; Chadwick et al., 2015; Suarez-Jimenez et al., 2018), the parietal cortex is considered to represent the egocentric space for both perception and memory.

Mnemonic representations of the egocentric space bring the question of whether the spatial representation differs between the inside and outside of a visual field. While the former can be represented in both vision and memory, the latter can be represented only in

memory. Previous human behavioral studies reported a decreased performance (Attneave, 1977) or prolonged response latency (Sholl, 1987) when participants located a target behind them. This phenomenon, known as "alignment effect" (Presson, 1984) or "front facilitation" (Kelly, 2009), suggests that the space surrounding our body is coded heterogeneously by different neural system depending on whether a target is inside or outside the visual field (Kelly, 2009). To explore the neural architectures responsible for the representation of egocentric space, previous studies mostly examined the target representation within the visual field; however, one previous neuroimaging study, which examined target representation outside the visual field, suggested that the parietal cortex codes unseen egocentric spaces (Schindler, 2013). However, the target representation of inside/outside of the visual field on the parietal cortex and its interactions with associated brain areas are still unsolved.

To characterize neural architectures supporting the mental representations of egocentric space inside and outside the visual field in the present study, we applied both functional magnetic resonance imaging (fMRI) and magnetoencephalography (MEG) to a spatial-memory paradigm using a 3D virtual environment for human participants, which we recently devised (Zhang and Naya, 2020) (Fig. 1a). In this paradigm, participants encoded a spatial relationship among three objects (walking period) in each trial. While the same three objects were used across trials, their spatial relationship was different in each trial. After the walking period, the participants faced one object (facing period), following a presentation of a target object (targeting period). The participants remembered the location of the target object relative to self-body. To-be-remembered targeting locations could be on the left, right, or back position of the participants' egocentric spaces. This spatial-memory paradigm allowed us to compare the neural representations of egocentric space between inside (i.e., left/right condition) and outside (i.e., back condition) of the visual field (Knapp, 1938).

# Materials and Methods

## Participants

Nineteen and twelve right-handed university students with normal or corrected-to-normal vision were recruited from Peking University for fMRI and MEG experiments, respectively (fMRI: 12 women, 7 men; MEG: 4 women, 8 men). The average ages of the participants recruited for fMRI and MEG experiments were 24.9 years (range: 18–30 years) and 22.5 years (range: 19–25 years), respectively. None of the participants had a history of psychiatric or neurological disorders; all of them provided written informed consent prior to the start of the experiment, which was approved by the Research Ethics Committee of Peking University.

## Experimental design

*Experimental design:* The details of the present design were described previously (Zhang and Naya, 2020). A 3D virtual environment was programmed using Unity platform (Unity Technologies, San Francisco). In the environment, three animate 3D human characters (Mixamo, San Francisco, https://www.mixamo.com) were placed on three out of four locations pseudo-randomly across trials (Fig. 1a). Participants performed the task using first-person perspective with a 90° field of view (aspect ratio = 4:3) and had never seen a top-down view of the virtual environment. Experimental stimuli were presented through an LCD projector with a resolution of 1024 × 768 pixels.

*Spatial-memory task:* The task included 144 and 72 trials in the MRI and MEG experiments, respectively. In each trial, participants walked from one of four starting locations toward the human characters and stopped at the center of a wood plate. After the walking period, participants experienced a “facing period” and a “targeting period” sequentially. In the facing period, one of the human characters was presented in the center of

the display with the environmental background for 2.0 s (MRI) or 1.0 s (MEG) as a facing-character with the other two characters being invisible. In the targeting period, a photo of one of the remaining characters (named as "targeting-character") was presented as a target on a scrabbled background for 2.0 s (MRI) or 1.0 s (MEG). Each of the three periods was followed by a 2.0 s (MRI) or 1.0 s (MEG) delay (noise screen). At the end of each trial, participants indicated the direction of the target relative to their self-body by pressing a button when a cue was presented.

We inserted head-nodding detection (HND) trials in the spatial-memory task (16 trials for MRI and 36 trials for MEG). In the HND trials, a photo of one of the human characters was presented after the walking period, and then the participants were asked to indicate whether the human character nodded its head or not during the walking period. Each human character nodded its head in a probability of 20.6% at a random time point between the start and end of walking in the HND trials. Because the trial-types were indistinguishable during the walking period, the participants were required to pay attention to the head-nodding of the human characters during the walking period, which would reduce the possibility of voluntary memorization of the spatial relationship of the three objects. Post-scanning interviews showed that none of the participants made efforts to memorize the spatial relationship (Zhang and Naya, 2020).

*MEG control conditions:* Two control conditions (36 trials for each) were added to the spatial-memory task in the MEG experiment. In the control conditions, after the walking period, a white cross was presented instead of a human character during both facing and targeting periods or during the targeting period (Fig. 4c). The participants were instructed to rest with eyes opened and fixate on the white cross. After the targeting period, the participants pressed the button corresponding to a number presented on the screen during the

response period. The number was determined randomly from 1 to 4 in each trial of the control conditions.

**fMRI acquisition and analysis**

*MRI scanning parameters:* Blood-oxygen-level-dependent (BOLD) MRI images were acquired using a 3T Siemens Prisma scanner equipped with a 20-channel receiver head coil. Functional data were acquired with a Multi-band Echo Planer imaging (EPI) sequence (TR: 2000 ms; TE: 30 ms; matrix size: 112 × 112 × 62; flip angle: 90°; gap: 0.3 mm; resolution: 2 × 2 × 2.3 $mm^3$; number of slices: 62; slice thickness: 2 mm; gap between slices: 0.3 mm; slice orientation: transversal). The signals of the original voxels (i.e., 2 × 2 × 2 $mm^3$) were assigned to the corresponding voxels without gap (2 × 2 × 2.3 $mm^3$) to construct participants' native space images. Four experimental sessions were conducted with average 478, 476, 473, and 475 TRs. A high-resolution T1-weighted three-dimensional anatomical data set was collected to aid registration (MPRAGE, TR: 2530 ms; TE: 2.98 ms; matrix size: 448 × 512 × 192; flip angle: 7°; resolution: 0.5 × 0.5 × 1 $mm^3$; number of slices: 192; slice thickness: 1 mm; slice orientation: sagittal).

*fMRI preprocessing:* BOLD images of each experimental session were preprocessed independently using FSL FEAT (FMRIB's Software Library, version 6.00, https://fsl.fmrib.ox.ac.uk/fsl/fslwiki; Woolrich et al., 2001; Woolrich et al., 2004). For each session, the first three functional volumes were discarded to allow for T1 equilibration, and the remaining functional volumes were slice-time corrected, realigned to the first image, high-pass filtered at 100 s, and smoothed using a 5-mm FWHM Gaussian filter.

*Univariate analysis:* The 4-s BOLD signals of the targeting period were modeled using univariate general linear models (GLM) with the three egocentric directions (left, right, back) included as regressors. To remove nuisance effects, an additional twenty-six regressors were

included: twelve for modeling the visual patterns of the walking period (3 spatial arrangements of human characters × 4 walking directions), four for the body turning-direction (turn left or turn right) and turning-angle (135° or 45) during the facing period, three for the response key pressed in the response period, one for HND trials, and six for motion parameters. This procedure generated three parameter maps of egocentric directions in participant's native space (2 × 2 × 2.3 mm voxels). For group-level statistical analysis, the activity parameter maps were averaged across four scanning sessions and registered to a T1-weighted standard image (MNI152) using FSL FLIRT (Jenkinson and Smith 2001; Jenkinson et al. 2002); this procedure also resampled the voxel size into the 2 × 2 × 2 $mm^3$ resolution before subjecting the data to two-tailed t-test.

*Connectivity analysis:* To examine the functional connectivity of the parietal cortex and precuneus inside and outside the visual field, a GLM was created to remove the nuisance covariates from the preprocessed functional data. The signal averaged over the lateral ventricles, white matter, and whole brain and six motion parameters, and their derivatives were specified as regressors. The residual signals were bandpass-filtered leaving signals within the frequency range of 0.01–0.1 Hz and shifted by two TR intervals (4 s) (Tompary and Davachi, 2017). The residual signals were registered to a T1-weighted standard image (MNI152) using FSL FLIRT (Jenkinson and Smith 2001; Jenkinson et al. 2002) with the voxel size resampled to a resolution of 2 × 2 × 2 $mm^3$. The regional time courses of targeting period were then extracted from the anatomical masks of the parietal cortex and precuneus on the basis of the AAL template (Rolls et al., 2015). To do this, we averaged signals over the mask at each TR within the period and then concatenated the two TRs in a trial with those in the next trial for each of the egocentric directions in a session (Ranganath et al., 2005, 24 TRs in total: 2 TRs × 12 trials). The regional time course was then correlated with the time course of each voxel in the rest of the brain, which yielded a whole-brain correlation map for inside

(left and right) and outside (back) of visual field separately. For group-level statistical analysis, the correlation maps were averaged across four scanning sessions before subjecting them to a two-tailed t-test.

**MEG acquisition and analysis**

*MEG scanning parameter:* Neuromagnetic signals were recorded with a 275-channel whole-head axial gradiometer MEG system DSQ-3500 (CTF MEG, Canada) at the sampling rate of 1200 Hz. A third-order synthetic gradiometer and linear drift corrections were applied to remove far-field noise. To measure head position within the MEG helmet, three head position indicator (HPI) coils were attached to the nasion and two preauricular points of each participant to coregister their head position with the sensor coordinate system. During scanning, a customized chin-rest equipment compatible with MEG was prepared to ensure that head movements did not exceed 2 mm. After MEG recording, each participant underwent anatomical MRI scans on a 3T Siemens Prisma scanner (voxel size: 1 $mm^3$; flip angle: 9; TE: 1.97 ms; TR: 2,300 ms; field of view: 256 × 256 × 176 $mm^3$); three MRI markers were attached to the same location of HPI coils to align each participant's anatomical image to the MEG sensor positions.

*MEG preprocessing:* The raw MEG data were preprocessed and analyzed using the MNE Python toolbox (v0.19; available at: https://mne.tools/stable/index.html)(Gramfort et al, 2013; Gramfort et al, 2014). The time series were bandpass-filtered between 1 and 100 Hz offline. To verify the data quality and remove artifacts, such as eye movements, eye blinks, and cardiac and environmental noises, independent component analysis (ICA) was performed, and visually inspection was applied after ICA artifact removal. The preprocessed time series were epoched from 0.2 s before the onset of targeting period to the end of subsequent noise

239 period (2.2 s duration) for each of left, right, back, and control conditions; the epochs were
240 downsampled to 200 Hz to increase the processing speed in later steps (Grenander, 1959).
241 *Sensor-space analysis:* From the neural activity indexed by the strength of magnetic field on
242 sensor space, the mean activity during the 0.2-s period preceding the onset of targeting period
243 in each trial was subtracted. To extract the difference in neural activity between the
244 egocentric location inside (left and right) and outside (back) the visual field of view, a
245 contrast analysis was performed between the mean of left/right condition and back condition
246 for each sensor. Another contrast analysis was performed to examine the main effect of the
247 three egocentric locations relative to the control conditions. The contrasted neural activity on
248 sensor space was then subjected to two-tailed t-test for group-level statistical analysis.
249 *Source space analysis:* To reconstruct the spatial-temporal activity from sensor space to
250 anatomical space, the forward model was created using single-compartment (inner skull)
251 boundary-element method (BEM) on the basis of each participant's anatomical image, and
252 the spatial-temporal activity was then inversely modeled using the dynamic statistical
253 parameter map in each source point and time (Dale et al., 2000). The source space was
254 estimated using a subsampling strategy, which involved subdividing a polygon (oct6) using
255 the spherical coordinate system provided by FreeSurfer, producing 4098 source points per
256 hemisphere with an average source spacing of 4.9 mm (assuming a surface area of 1000
257 $cm^2$/hemisphere)(Fischl et al., 1999; Gramfort et al., 2013). Noise covariance matrix was
258 derived from the baseline period (−0.2 s to 0 s relative to targeting period). The source space
259 of each participant was morphed to an fsaverage surface before submitting to group-level
260 statistical analysis. The percentile rank of source-power strength from top 5% to 1% was
261 calculated for either each of egocentric locations or the contrast between the left/right and
262 back. For ROI analysis, we manually delineated each of the medial temporal lobe (MTL)
263 subareas (HPC, PHC, PRC, ERC) on participant's native space using established protocols

(Insausti et al., 1998; Pruessner et al., 2000; Pruessner et al., 2002; Duvernoy, 2005) as well as the delineating software ITK-SNAP (www.itksnap.org). The mean source-power within the MTL subareas was calculated by averaging the source-power within each mask for each of egocentric locations before subjecting the data to group-level statistical analysis.

*Connectivity analysis:* To access the connectivity of the parietal cortex and precuneus with the frontal lobe (FEF/SMA) and MTL subareas in each temporal domain revealed by the MEG contrast analysis [i.e., 'early' (0.25-0.37 s after the onset of targeting period) for the back and 'late' (0.67-0.85 s) for the left/right], we examined the phase synchronization of MEG time series for the following four frequency bands: alpha (8-13 Hz), beta (13-30 Hz), low-gamma (30-60 Hz), and high-gamma (60-99 Hz) bands. We extracted the MEG time series using a 400 ms time windows for each of the "early" and "late" periods to ensure that at least three cycles of source time series could be covered in alpha band (Hu and Zhang, 2019). To do so, we first calculated powers of the MEG signal using all frequency bands in the time windows of 400 ms centering on the time points within the two time periods. We then selected a time window that had the maximum power for each time period. This procedure resulted in two time series (0.08-0.48 s and 0.56-0.96 s for the "early" and "late" periods, respectively). The phase synchronization was tested among the eight ROIs (parietal cortex, precuneus, FEF, SMA, and right MTL subareas) for each time series, condition (left, right or back), and frequency band using phase lag index (PLI) (Stam et al., 2007; Colclough et al., 2016) and the built-in function of MNE Python toolbox (Gramfort et al, 2013; Gramfort et al, 2014). Subsequently, the connectivity contrast analysis ("back"–"left/right") was performed before subjecting the data to group-level statistical analysis.

**Statistical analysis**

An initial threshold of $P < 0.01$ was applied to the whole-brain statistics of MRI univariate and connectivity analyses. The reliability of clusters was tested using a nonparametric statistical inference that does not make assumptions about the distribution of the data (Nichols and Holmes, 2002; Winkler et al., 2014; Chadwick et al., 2015), The test was conducted with the FSL randomize package (version v2.9, http://fsl.fmrib.ox.ac.uk/fsl/fslwiki/Randomise), with 5000 random sign-flips; we then reported clusters with a size higher than 95% of the maximal suprathreshold clusters in permutation distribution. Data obtained by ROI analysis of MRI BOLD signal, MEG source-power, and MEG connectivity analysis were tested using either repeated-measures ANOVA or *t*-test. The MEG sensor space analysis used either spatial-temporal cluster permutation test or spatial cluster permutation test. All statistical tests were two-sided unless otherwise noted and the significance was determined according to whether the corrected *P* value was smaller than 0.05.

# Results

## Behavioral performance in the spatial-memory task

Nineteen and twelve healthy volunteers participated in the fMRI and MEG experiments, respectively. The performances in the spatial-memory task exhibited a ceiling effect in both the experiments (MRI: 93.6% ± 1.5%; MEG: 90.4% ± 1.9%) (Fig. 1c). The performances did not differ among the three target locations (i.e., right, left, and back) in the fMRI [$F(2,54) = 0.82$, $P = 0.44$] and MEG [$F(2,33) = 0.08$, $P = 0.93$] experiments. These behavioral results indicated that the participants solved the spatial-memory task accurately in both fMRI and MEG experiments regardless of the target location in the present study.

## MRI contrast analysis between left/right and back-target location

The neural activity in the fMRI experiment was examined using the 2 s time-window of the targeting period in which the participants remembered the location of a targeting object (i.e., human character) relative to their self-body in the virtual environment. We first investigated the brain regions that represented the egocentric location of the target object, when it was inside and outside the visual field, by comparing the mean BOLD signal strengths for the left and right-target locations (left/right condition) with that for the back-target location (back condition). A contrast analysis showed a significantly stronger BOLD signal for the left/right-target location than for the back-target location in the parietal cortex, precuneus, frontal eye field (FEF), and supplementary motor area (SMA) (Fig. 2a, $P < 0.01$, initial threshold, $P < 0.05$, cluster-corrected for multiple comparison). In contrast, no brain region showed a BOLD signal for the back-target location that was significantly larger than that shown by any brain region for the left/right-target location even with the use of a more liberal threshold of statistical significance ($P < 0.05$, uncorrected).

The BOLD signal during the targeting period was further examined for each of the right, left, and back-target locations in each hemisphere of the parietal cortex, precuneus, FEF, and SMA separately using the eight functional ROIs derived from the contrast analysis in Fig. 2a (i.e., 2 hemispheres, 4 regions, and 3 egocentric locations). The results showed significant BOLD signal changes across the three target locations for all ROIs ($P < 0.05$, repeated-measures one-way ANOVA, Bonferroni-corrected for multiple comparisons among the brain regions, $n = 2 \times 4 = 8$). In addition, for all ROIs, a significantly weaker BOLD signal was found for the back-target condition than for either the left-target or right-target condition (Fig. 2b, $P < 0.05$, paired $t$-test, Bonferroni-corrected for multiple comparison among combination of the conditions, $n = 3$). The elevated activities in the left and right conditions indicate that involvements of those dorsal brain areas in processing a target in the visual field were greater than those involved in processing the target outside of it although the participants did not perceive the target location directly under the left/right-target (inside of the visual field) or back-target condition (outside of the visual field). In addition to the strong activity bias for the target inside the visual field, the left FEF and bilateral SMA showed significantly different strengths of BOLD signals between the left-target and right-target conditions [Fig. 2b, the left FEF: $t(18) = 3.79$, $P = 0.01$, the left SMA: $t(18) = 5.50$, $P = 0.0002$, the right SMA: $t(18) = 4.46$, $P = 0.002$, Bonferroni-corrected for multiple comparison, $n = 8$]. In contrast with the FEF and SMA, neither the parietal cortex nor precuneus revealed significant differences in BOLD signal strengths between the left-target and right-target conditions even when a liberal threshold was used ($P < 0.05$, uncorrected). These results might reflect the distinction in the functions of the frontal lobe (FEF and SMA) and parietal lobe (parietal cortex and precuneus) with regard to processing egocentric information. The former might be involved in an action planning (Tanji and Shima, 1994; Schall et al., 1995; Hanes et al., 1995;

Amador and Fried, 2004), while the latter might be associated with a spatial representation (Colby et al., 1995; Merriam et al., 2003).

**MRI functional-connectivity analysis**

We subsequently investigated the brain regions that interacted with the parietal cortex and precuneus for representing an egocentric location of a target object, when it was inside and outside the visual field. To examine the interactions, we conducted whole-brain functional-connectivity analysis under the left/right-target and back-target conditions by using the anatomical ROIs of the parietal cortex and precuneus as the seeds based on the automated anatomical labeling (AAL) (see method for details). The whole-brain functional-connectivity analysis showed that, in addition to a mutual connectivity between these brain areas, both the parietal cortex and precuneus exhibited a significantly higher connectivity to the FEF and SMA under the left/right-target condition than under the back-target condition (Fig. 3a, $P < 0.01$, initial threshold, $P < 0.05$, cluster-corrected for multiple comparison). This result indicates the preferential involvements of the FEF, SMA, parietal cortex, and precuneus for processing a target object in the visual field even though the egocentric object location was not perceived. In contrast, the parietal cortex but not the precuneus increased the functional connectivity to the right ERC when a retrieved target location was beyond the visual field (i.e., back condition) (Fig. 3b, $P < 0.01$, initial threshold, $P < 0.05$, cluster-corrected for multiple comparison) although the ERC cluster survived only for a small volume correction based on the mask for the MTL. We also examined the functional connectivity using the FEF and SMA seeds and found that these two brain regions exhibited a strong connectivity to the parietal cortex and precuneus in the left/right-target condition but did not increase functional connectivity to any other brain regions, including the ERC, in the back-target condition. These results suggest that a brain network consisting of the parietal cortex and ERC

374 represents a target object beyond the visual field, which is distinct from the other brain
375 network consisting of the FEF, SMA, precuneus, and parietal cortex that represents a target
376 object in the visual field.
377
378 **MEG temporal-spatial analysis**
379 Although the functional connectivity analysis suggests the occurrence of coupling between
380 the ERC and parietal cortex for the target representation outside the visual field, an increase
381 in BOLD signal strength was not detected in the ERC for the back-target condition. One
382 possible reason behind this result is that the ERC is involved in representing a target outside
383 the visual field more than inside for only a short duration, which might make it difficult for
384 the present fMRI study to detect the effect. To address this problem, we conducted a MEG
385 study using the same spatial-memory task that was used for the fMRI study except for the
386 time parameters (Fig. 1a).
387 Figure 4a shows the results of contrast analysis that compared the activity strength at
388 each sensor between the left/right-target and back-target conditions after the onset of
389 targeting period. We found a cluster of sensors in the left-posterior area, which showed
390 significantly stronger activity under the left/right-target condition than under the back-target
391 condition during 0.67–0.85 s after the onset of targeting period ($P < 0.05$, initial threshold,
392 two tailed; $P = 0.04$, spatial-temporal cluster-corrected for multiple comparison) (Fig. 4b).
393 Conversely, no cluster of sensors showed stronger activity under the back-target condition
394 than under the left/right-target condition. These MEG results were consistent with those of
395 the fMRI contrast analysis and suggest the predominant spatial-representation processing
396 within the visual field relative to that outside the visual field.
397 We subsequently examined the effect of egocentric target location by comparing the
398 activity strength under back-target, left-target, and right-target conditions with the control

399 trials, in which a targeting character was not presented and the participants were not required
400 to remember a target location (Fig. 4c). Figure 4d shows the time course of the topographic
401 activity map and the activity strengths under each condition relative to those under the
402 control conditions. An increased activity was observed on the left-posterior area of the head.
403 This left-posterior cluster showed a significant increase in activity during 0.5–0.6 s from the
404 onset of targeting period under the left-target and right-target conditions ($P < 0.05$, initial
405 threshold; $P < 0.05$, cluster-corrected for multiple comparison) although the same trend of
406 increase in activity was observed under the back-target condition [$t(11) = 2.42$, $P = 0.03$,
407 uncorrected]. To localize the brain regions contributing to the significant activity increase on
408 the left-posterior cluster, we conducted the source analysis of MEG signal (Dale et al., 2000).
409 The source powers were distributed largely in the parietal cortex and precuneus for the left-
410 target and right-target conditions (Fig. 4e). We also found the source-power for the back-
411 target condition to be distributed in the parietal cortex and precuneus although the level of
412 source-power was smaller than those under the left-target and right-target conditions.
413 To explore the brain regions exhibiting larger neural activity under the back-target
414 condition than under the left/right-target condition, we conducted a whole-brain analysis to
415 compare the source-power between the two conditions, every 0.2 s after the onset of targeting
416 period (Fig. 5a). We found a strong source-power for the back-target condition in the right
417 MTL including the ERC during 0.2–0.4 s after the onset of targeting period. Using
418 anatomical ROIs of each hemisphere of the whole MTL, we examined a precise time course
419 of the source-power for the back-target and left/right-target conditions separately, relative to
420 the control trials. The result indicated elevations in the source-power after the onset of
421 targeting period under both back-target and left/right-target conditions relative to the control
422 condition in both hemispheres of the MTL. However, only the right MTL exhibited a
423 significantly larger source-power for the back-target condition than for the left/right-target

condition in the early phase (0.25-0.37 s) after the onset of targeting period (Fig. 5b, $P < 0.05$, initial threshold; $P < 0.05$, spatial-temporal cluster correction for multiple comparison, two tailed). We further examined the source-power in the right MTL using the anatomical masks of its subregions and found that the source-power was larger under the back-target condition than under the left/right-target condition in all the subregions [HPC: $t(11) = 3.00$, $P = 0.048$; PHC: $t(11) = 2.98$, $P = 0.049$; PRC: $t(11) = 3.22$, $P = 0.032$; ERC: $t(11) = 3.39$, $P = 0.024$, Bonferroni-corrected for multiple comparisons (n = 4)] (Fig. 5c). Collectively, the MEG source-power contrast analyses between the back-target and left/right-target conditions indicate that the right MTL including the ERC was involved more under the back-target condition than under the left/right-target condition in the early phase (0.25-0.37 s) after the onset of targeting period, while the parietal cortex and precuneus were involved more under the left/right-target condition than under the back-target condition in the late phase (0.67-0.85 s).

We examined the connectivity of the parietal cortex with the FEF, SMA, and MTL areas by calculating PLI using the MEG data (Stam et al., 2007). We chose the two time-windows of interests (0.08-0.48 s and 0.56-0.96 s after the onset of targeting period, see method for details) that covered the early and late phases and were revealed from the MEG source-power contrast analysis (Figs, 4&5), and subsequently, we included at least three cycles of alpha-band waves. Figure 6 shows the differences in the connectivity between the back-target and left/right-target conditions. The connectivity patterns differed significantly between the two time-windows in alpha band (8-13 Hz) but not in other bands [($F(1, 132) = 8.24$, $P = 0.02$, repeated-measures two-way ANOVA, Bonferroni-corrected for multiple comparisons, n = 4 for frequency bands]. During the early time window, the parietal cortex showed a larger connectivity with the right ERC and PRC of the MTL under the back-target condition than under the left/right-target condition although it was statistically marginal

449 (ERC: t(11) = 2.16, P = 0.06; PRC: t(11) = 1.91, P = 0.08, uncorrected). Conversely, we
450 found a larger connectivity of the parietal cortex with the FEF (t(11) = 2.61, P = 0.02,
451 uncorrected) and SMA (t(11) = 1.73, P = 0.11, uncorrected) under the left/right-target
452 condition than under the back-target condition during the late time window. These results
453 were consistent with those of the functional connectivity analysis of fMRI (Fig. 3). In
454 contrast with that in the case of the parietal cortex, we did not find a change in the
455 connectivity of the precuneus with any of the ROIs in any frequency band across the two
456 time-windows of interests.

# Discussion

The present combined fMRI and MEG study showed the larger involvements of the parietal cortex and its associated frontal areas (i.e., FEF and SMA) in the representations of target object within the visual field than outside the visual field although the egocentric spatial information was retrieved from short-term memory in both conditions and did not depend on the incoming visual sensory signal. Conversely, a larger interaction of the parietal cortex with the MTL including the ERC was revealed by both fMRI and MEG experiments, when a target object was behind a participant, although an increasing activity of the MTL was detected by only the MEG experiment with a high temporal resolution. These results suggest the two distinct networks that represent the egocentric space inside or outside the visual field (Fig. 7).

Results of both fMRI and MEG experiments exhibited disproportional spatial representations around the self-body, which showed a stronger bias toward a target object within the visual field than that behind the self-body. Preferential processing of a target location within the visual field by the fronto-parietal network may be consistent with the results of previous behavioral studies reporting “front facilitation”, i.e., location of a target in front of a participant is more efficiently detected than that located behind them (Attneave, 1977; Sholl, 1987; Kelly, 2009).

One previous human fMRI study using multi-voxel pattern analysis (MVPA) reported that the parietal cortex codes the egocentric space both inside and outside of the visual field (Schindler and Barteles, 2013), which is consistent with the finding of our previous MVPA-based study that employed the same spatial-memory task as did the present one (Zhang and Naya, 2020). However, Schindler and Barteles (2013) did not find a relationship between mean BOLD signal strength and egocentric space that was demonstrated by the present study. The reason behind this discrepancy might be difference in the type of memory engaged in

482 locating a target object between the two studies. Schindler and Barteles (2013) intensively
483 trained participants for several days before the MRI scanning as they could remember the
484 location of the target object from the long-term memory, which stored the fixed spatial
485 relationship among eight objects. On the contrary, the present study prompted the participants
486 to encode the spatial relationship of the objects involuntarily in each trial (see Methods) and
487 remember the target location from the short-term memory. The distinct memory properties
488 between the two studies (i.e., 'long-term memory & voluntary encoding' and 'short-term
489 memory & involuntary encoding') may differentiate participants' retrieval strategies, which
490 may affect the representation of egocentric space in each study.

491 While the fronto-parietal network represents the target within the visual field, the
492 MTL-parietal network was more involved in the spatial representations outside the visual
493 field. However, it may also be important to note that the MEG source-power increased in the
494 MTL for targets both inside and outside of the visual field (Figs. 5b&c). These results suggest
495 the spreading of retrieved information from the MTL to parietal lobe (e.g., precuneus and
496 parietal cortex), when the participants remembered a target location either inside or outside of
497 the visual field. The spreading of memory retrieval signal from the MTL to the parietal lobe
498 may be supported by the early increase in the MEG source-power in the MTL (Fig. 5b) (Naya
499 et al., 2001). These findings are consistent with those of previous studies, which suggest
500 involvements of the parietal cortex and precuneus in the recollection of episodic memory as
501 members of the core brain system, which also includes the MTL (Schacter et al., 2007; Byrne
502 et al., 2007).

503 The preferred involvement of the MTL-parietal network in the mental representation
504 of the back space was supported by the fMRI connectivity analysis (Fig. 3b) in addition to the
505 MEG study. However, only the ERC coupled with the parietal cortex in the fMRI study while
506 the MEG study suggested the involvements of other MTL subregions in addition to the ERC.

This inconsistency might be due to the ill-posed nature of the MEG inverse problem (e.g. the "source leakage"), considering that a limited number of magnetic-field sensors yielded insufficient activity that discriminated among thousands of source points particularly for neighboring regions (de Peralta-Menendez and Gonzalez-Andino, 1998; Sato et al., 2004; Colclough et al., 2015). The MEG source-power in the other MTL subregions might thus be caused by the signal leakage from the ERC. Another possibility might be that the MEG signal reflected synchronized activity at each instantaneous time point and would be more sensitive to the transient neuronal operation than is the fMRI connectivity analysis, which is based on the averaged BOLD signal (Logothetis et al., 2001) in each TR (2 s). In either case, the ERC might play a key role in the MTL-parietal network for the representation of a retrieved target location, which is consistent with the results of previous studies that examined response properties of the ERC neurons (e.g., grid cells, head direction cells) in both rodents (Hafting, et al, 2005; Hargreaves et al., 2005; Howard et al. 2014; Chadwick et al. 2015; Wang et al, 2018) and primates (Doeller et al., 2010; Killian et al., 2012; Wilming et al., 2018). Importantly, the primate ERC reportedly represents the external space according to the gaze position and even in imagined navigation (Horner et al., 2016). In contrast to the ERC, other MTL subregions might be involved in the retrieval of the target location (Yang and Naya, 2020). Considering the high performance of the present spatial-memory task and the post-scan interview showing no strategic retrieval efforts by the participants, the retrieval process might only be transient in the present experimental paradigm, which could be detected more efficiently by MEG than by fMRI.

MEG connectivity analysis using PLI revealed the preferential increase in synchronization at alpha-band frequency (8-13 Hz) for both fronto-parietal and MTL-parietal networks inside and outside of the visual field, respectively. These findings were consistent with previous MEG and EEG studies, which suggest functional roles of alpha-band phase

532 synchrony in long-range communications across distant brain regions including the parietal
533 cortex (Desburg et al., 2009; Sadaghiani et al., 2012; Takahashi and Kitazawa, 2017; Lobier
534 et al., 2018). One remaining question is that of the functional significance of increased
535 involvements of the MTL-parietal network in the representation of a retrieved target behind
536 the participants. In the present spatial-memory paradigm, the participants obtained the
537 egocentric location of a target located either inside or outside of the visual field from their
538 short-term memory (Zhang and Naya 2020). It should be noted here that the task required the
539 participants to identify the location of the target object that was present around them in the
540 virtual environment. In our daily life, we usually perceive and attend targets within the visual
541 field for the subsequent action (Ohbayashi et al., 2003 Science) while we, sometimes, retrieve
542 a target behind us from short-term memory, the contents of which have already passed by in
543 our spatiotemporal space (Naya and Suzuki, 2011; Eichenbaum, 2014; Tsao et al., 2018) (Fig.
544 7). We may thus combine the back scene, which we encoded just before retrieval, with the
545 mental representation of the present external world. This assumption suggests that the MTL-
546 parietal network may serve more for the representation of the back space than for that of the
547 front space although future studies should elucidate additional neuronal operations required
548 for representing the scene behind self-body. Collectively, our results indicate that the parietal
549 cortex may represent the whole space around self-body by coordinating the fronto-parietal
550 network for the target inside and the MTL-parietal network for the target outside the visual
551 field, corresponding to the future and past relative to the present time point.

552 # Reference

553

554 Attneave F, Farrar P (1977) The visual world behind the head. Am J Psychol
555 90:549–563.

556

557 Amador N, Fried I (2004) Single-neuron activity in the human supplementary motor
558 area underlying preparation for action. J Neurosurg 100:250–259.

559

560 Burgess N (2006) Spatial memory: how egocentric and allocentric combine. Trends
561 Cogn Sci 10:551–557.

562

563 Bisiach E, Luzzatti C (1978) Unilateral neglect of representational
564 space. Cortex 14:129–133.

565

566 Byrne P, Becker S, Burgess N (2007) Remembering the past and imagining the
567 future: a neural model of spatial memory and imagery. Psychol Rev 114:340–375.

568

569 Chadwick MJ, Jolly AE, Amos DP, Hassabis D, Spiers HJ (2015) A goal direction
570 signal in the human entorhinal/subicular region. Curr Biol 25:87–92.

571

572 Colclough GL, Woolrich MW, Tewarie PK, Brookes MJ, Quinn AJ, Smith SM (2016)
573 How reliable are MEG resting-state connectivity metrics? Neuroimage 138:284–293.

574

575 Ciaramelli E, Rosenbaum RS, Solcz S, Levine B, Moscovitch M (2010) Mental space
576 travel: damage to posterior parietal cortex prevents egocentric navigation and
577 reexperiencing of remote spatial memories. J Exp Psychol Learn Mem Cogn 36:619.
578
579 Colby CL, Duhamel JR, Goldberg ME (1995) Oculocentric spatial representation in
580 parietal cortex. Cereb Cortex 5:470–481.
581
582 Colclough GL, Brookes MJ, Smith SM, Woolrich MW (2015) A symmetric
583 multivariate leakage correction for MEG connectomes. Neuroimage 117:439–448.
584
585 Dale AM, Liu AK, Fischl BR, Buckner RL, Belliveau JW, Lewine JD, Halgren E (2000)
586 Dynamic statistical parametric mapping: combining fMRI and MEG for high-
587 resolution imaging of cortical activity. Neuron 26:55–67.
588
589 Doesburg SM, Green JJ, McDonald JJ, Ward LM (2009) From local inhibition to
590 long-range integration: a functional dissociation of alpha-band synchronization
591 across cortical scales in visuospatial attention. Brain Res 1303:97–110.
592
593 Desmurget M, Epstein CM, Turner RS, Prablanc C, Alexander GE, Grafton ST (1999)
594 Role of the posterior parietal cortex in updating reaching movements to a visual
595 target. Nat Neurosci 2:563–567.
596
597 Donner T, Kettermann A, Diesch E, Ostendorf F, Villringer A, Brandt SA (2000)
598 Involvement of the human frontal eye field and multiple parietal areas in covert visual
599 selection during conjunction search. Eur J Neurosci 12:3407–3414.

Duvernoy HM (2005) The human hippocampus: functional anatomy, vascularization and serial sections with MRI. New York, NY: Springer Science & Business Media.

de Peralta-Menendez RG, Gonzalez-Andino SL (1998) A critical analysis of linear inverse solutions to the neuroelectromagnetic inverse problem. IEEE Trans Biomed Eng 45:440–448.

Doeller CF, Barry C, Burgess N (2010) Evidence for grid cells in a human memory network. Nature 463:657–661.

Eichenbaum H, Cohen NJ (2014) Can we reconcile the declarative memory and spatial navigation views on hippocampal function? Neuron 83:764–770.

Fischl B, Sereno MI, Tootell RB, Dale AM (1999) High-resolution intersubject averaging and a coordinate system for the cortical surface. Hum Brain Mapp 8:272–284.

Gramfort A, Luessi M, Larson E, Engemann DA, Strohmeier D, Brodbeck C, Goj R, Jas M, Brooks T, Parkkonen L, Hämäläinen M (2013) MEG and EEG data analysis with MNE-Python. Front Neurosci 7:267.

Gramfort A, Luessi M, Larson E, Engemann DA, Strohmeier D, Brodbeck C, Parkkonen L, Hämäläinen MS (2014) MNE software for processing MEG and EEG data. Neuroimage 86:446–460.

Goodale MA, Milner AD (1992) Separate visual pathways for perception and action. Trends Neurosci 15:20–25.

Grenander U (1959) Probability and Statistics: The Harald Cramér Volume. New York, NY: Almqvist & Wiksell.

Hu L, Zhang Z (2019) EEG Signal Processing and Feature Extraction. Singapore: Springer Singapore.

Hanes DP, Thompson KG, Schall JD (1995) Relationship of presaccadic activity in frontal eye field and supplementary eye field to saccade initiation in macaque: Poisson spike train analysis. Exp Brain Res 103:85–96.

Hafting T, Fyhn M, Molden S, Moser MB, Moser EI (2005) Microstructure of a spatial map in the entorhinal cortex. Nature 436:801–806.

Hargreaves EL, Rao G, Lee I, Knierim JJ (2005) Major dissociation between medial and lateral entorhinal input to dorsal hippocampus. Science 308:1792–1794.

Horner AJ, Bisby JA, Zotow E, Bush D, Burgess N (2016) Grid-like processing of imagined navigation. Curr Biol 26:842–847.

Insausti R, Juottonen K, Soininen H, Insausti AM, Partanen K, Vainio P, Laakso MP, Pitkänen A (1998) MR volumetric analysis of the human entorhinal, perirhinal, and temporopolar cortices. AJNR Am J Neuroradiol 19:659–671.

Jenkinson M, Smith S (2001) A global optimisation method for robust affine registration of brain images. Med Image Anal 5:143–156.

Jenkinson M, Bannister P, Brady M, Smith S (2002) Improved optimization for the robust and accurate linear registration and motion correction of brain images. Neuroimage 17:825–841.

Knapp A (1938) An Introduction to Clinical Perimetry. Arch Ophthalmol 20:1116–1117.

Kelly JW, McNamara TP (2009) Facilitated pointing to remembered objects in front: Evidence for egocentric retrieval or for spatial priming? Psychon Bull Rev 16:295–300.

Killian NJ, Jutras MJ, Buffalo EA (2012) A map of visual space in the primate entorhinal cortex. Nature 491:761–764.

Khan AZ, Blangero A, Rossetti Y, Salemme R, Luauté J, Deubel H, Schneider WX, Laverdure N, Rode G, Boisson D, Pisella L (2008) Parietal damage dissociates saccade planning from presaccadic perceptual facilitation. Cereb Cortex 19:383–387.

Lobier M, Palva JM, Palva S (2018) High-alpha band synchronization across frontal, parietal and visual cortex mediates behavioral and neuronal effects of visuospatial attention. Neuroimage 165:222–237.

Logothetis NK, Pauls J, Augath M, Trinath T, Oeltermann A (2001) Neurophysiological investigation of the basis of the fMRI signal. Nature 412:150–157.

Iriki A, Taoka M (2012) Triadic (ecological, neural, cognitive) niche construction: a scenario of human brain evolution extrapolating tool use and language from the control of reaching actions. Philos Trans R Soc Lond B Biol Sci 367:10–23.

Merriam EP, Genovese CR, Colby CL (2003) Spatial updating in human parietal cortex. Neuron 39:361–373.

Nichols TE, Holmes AP (2002) Nonparametric permutation tests for functional neuroimaging: a primer with examples. Hum Brain Mapp 15:1–25.

Presson CC, Hazelrigg MD (1984) Building spatial representations through primary and secondary learning. J Exp Psychol Learn Mem Cogn 10:716–722.

Pruessner JC, Li LM, Serles W, Pruessner M, Collins DL, Kabani N, Lupien S, Evans AC (2000) Volumetry of hippocampus and amygdala with high-resolution MRI and three-dimensional analysis software: minimizing the discrepancies between laboratories. Cereb Cortex 10:433–442.

Pruessner JC, Köhler S, Crane J, Pruessner M, Lord C, Byrne A, Kabani N, Collins DL, Evans AC (2002) Volumetry of temporopolar, perirhinal, entorhinal and

parahippocampal cortex from high-resolution MR images: considering the variability of the collateral sulcus. Cereb Cortex 12:1342–1353.

Rolls ET, Joliot M, Tzourio-Mazoyer N (2015) Implementation of a new parcellation of the orbitofrontal cortex in the automated anatomical labeling atlas. Neuroimage 122:1–5.

Stein JF (1989) Representation of egocentric space in the posterior parietal cortex. Q J Exp Physiol 74:583–606.

Stein JF (1992) The representation of egocentric space in the posterior parietal cortex. Behav Brain Sci 15:691–700.

Sadaghiani S, Scheeringa R, Lehongre K, Morillon B, Giraud AL, D'Esposito M, Kleinschmidt A (2012) Alpha-band phase synchrony is related to activity in the fronto-parietal adaptive control network. J Neurosci 32:14305–14310.

Sholl MJ (1987) Cognitive maps as orienting schemata. J Exp Psychol Learn Mem Cogn 13:615–628.

Shelton AL, McNamara TP (1997) Multiple views of spatial memory. Psychon Bull Rev 4:102–106.

Schindler A, Bartels A (2013) Parietal cortex codes for egocentric space beyond the field of view. Curr Biol 23:177–182.

Suarez-Jimenez B, Bisby JA, Horner AJ, King JA, Pine DS, Burgess N (2018) Linked networks for learning and expressing location-specific threat. Proc Natl Acad Sci U S A 115:E1032–E1040.

Stam CJ, Nolte G, Daffertshofer A (2007) Phase lag index: assessment of functional connectivity from multi channel EEG and MEG with diminished bias from common sources. Hum Brain Mapp 28:1178–1193.

Sato MA, Yoshioka T, Kajihara S, Toyama K, Goda N, Doya K, Kawato M (2004) Hierarchical Bayesian estimation for MEG inverse problem. Neuroimage 23:806–826.

Tanji J, Shima K (1994) Role for supplementary motor area cells in planning several movements ahead. Nature 371:413–416.

Takahashi T, Kitazawa S (2017) Modulation of illusory reversal in tactile temporal order by the phase of posterior α rhythm. J Neurosci 37:5298–5308.

Ungerleider LG, Haxby JV (1994) 'What' and 'where' in the human brain. Curr Opin Neurobiol 4:157–165.

Vallar G (1998) Spatial hemineglect in humans. Trends Cogn Sci 2:87–97.

Wilming N, König P, König S, Buffalo EA (2018) Entorhinal cortex receptive fields are modulated by spatial attention, even without movement. Elife 7:e31745.

Wang X, Fung CA, Guan S, Wu S, Goldberg ME, Zhang M (2016) Perisaccadic receptive field expansion in the lateral intraparietal area. Neuron 90:400–409.

Yang C, Naya Y (2020) Hippocampal cells integrate past memory and present perception for the future. BioRxiv doi: https://doi.org/10.1101/2020.03.08.982355

Zhang B, Naya Y (2020) Medial prefrontal cortex represents the object-based cognitive map when remembering an egocentric target location. Cereb Cortex bhaa117.

Zhou Y, Friston KJ, Zeidman P, Chen J, Li S, Razi A (2018) The hierarchical organization of the default, dorsal attention and salience networks in adolescents and young adults. Cereb Cortex 28:726–737.

766 **Figure Legends**

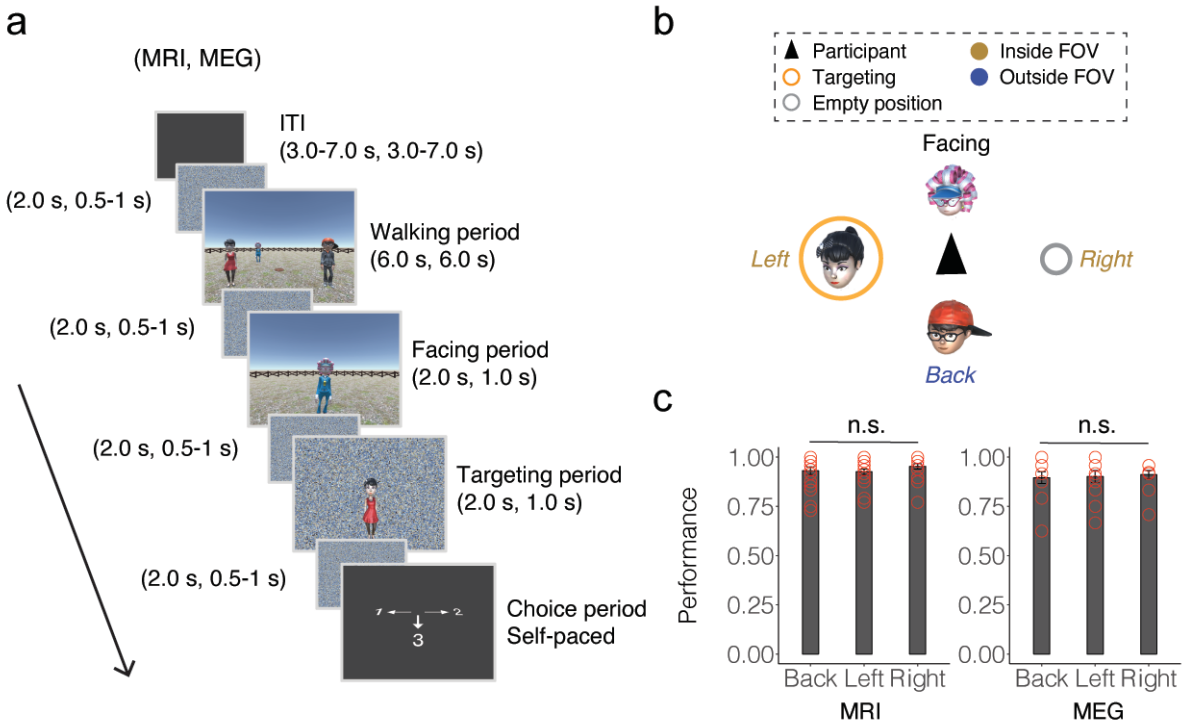


767

768 Figure 1. a) Spatial-memory task paradigm. Each trial consisted of four periods. Walking
769 period: participants walked toward three human characters using the first-person perspective
770 and stopped on a wood plate in the center. Facing period: one of the human characters was
771 presented, indicating the participant's current self-orientation. Targeting period: a photo of
772 target character was presented on the scrambled background. Choice period: the participants
773 chose the direction of the target character relative to their body upon the presentation of a
774 response cue. b) An example of the spatial relationship between a participant and the human
775 characters. Left-target and right-target conditions (yellow) are inside the visual field. Back-
776 target condition (blue) is outside the visual field. c) Performance of participants with regard
777 to the three egocentric directions in MRI and MEG experiments. Error bar indicates SEM.
778 n.s., no statistical significance detected by repeated-measures one-way ANOVA.

779

780

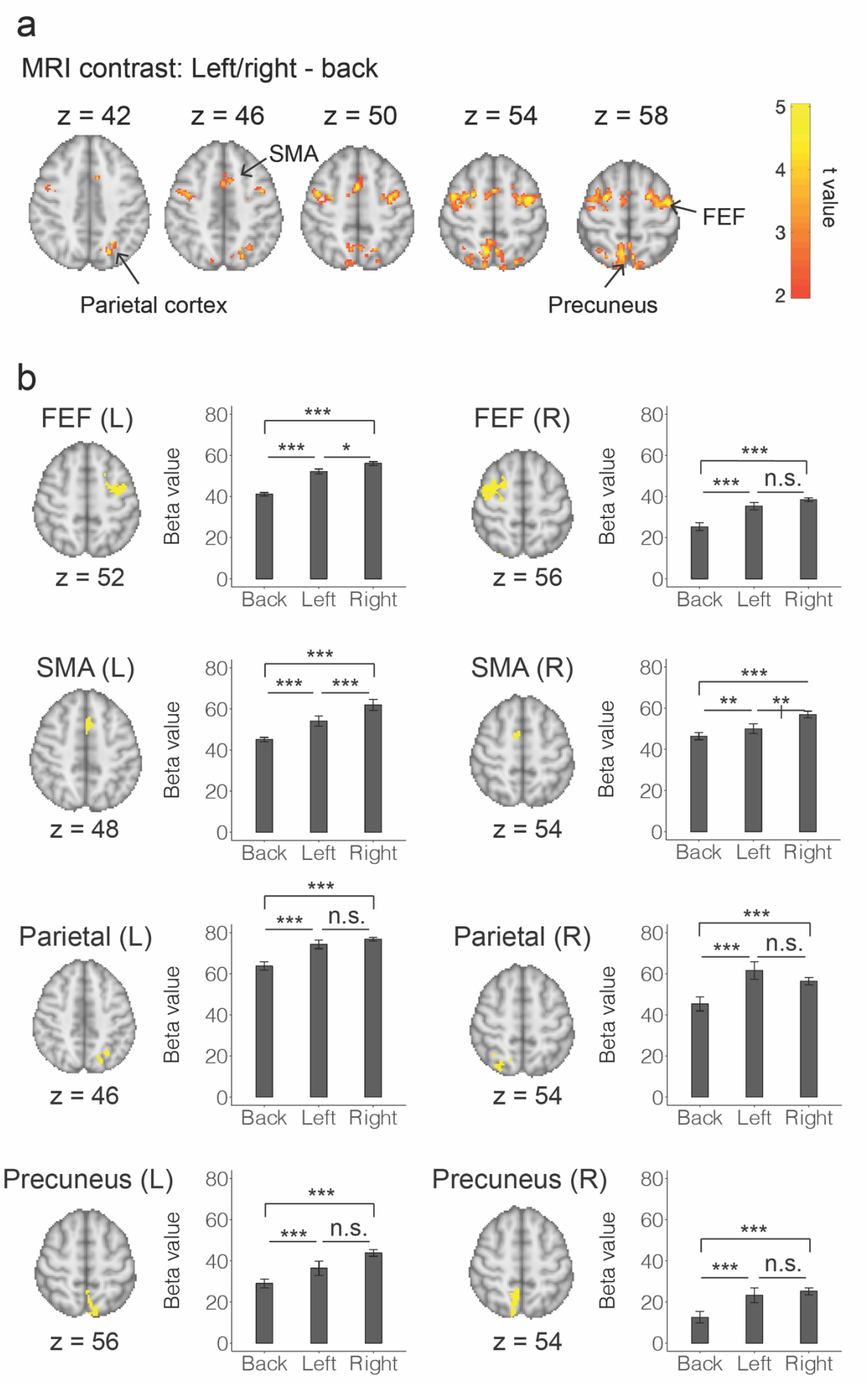

Figure 2. a) MRI contrast left/right–back condition: significant clusters were revealed in the parietal cortex, precuneus, FEF, and SMA, while no significant cluster was found for the back-target condition relative to the left/right-target condition (cluster-corrected for multiple comparison, initial threshold $P = 0.01$). b) BOLD signal in the functional ROIs derived from Fig. 2a for each of the left-target, right-target, and back-target conditions. All ROIs showed significant BOLD signal changes across the three conditions according to repeated-measures one-way ANOVA ($P < 0.05$, Bonferroni-corrected for multiple comparisons for the ROIs, n = 8). * $P < 0.05$, ** $P < 0.01$, *** $P < 0.001$, two-tailed t-test, Bonferroni-corrected for multiple comparisons for the conditions (n = 3). Error bar indicates SEM.

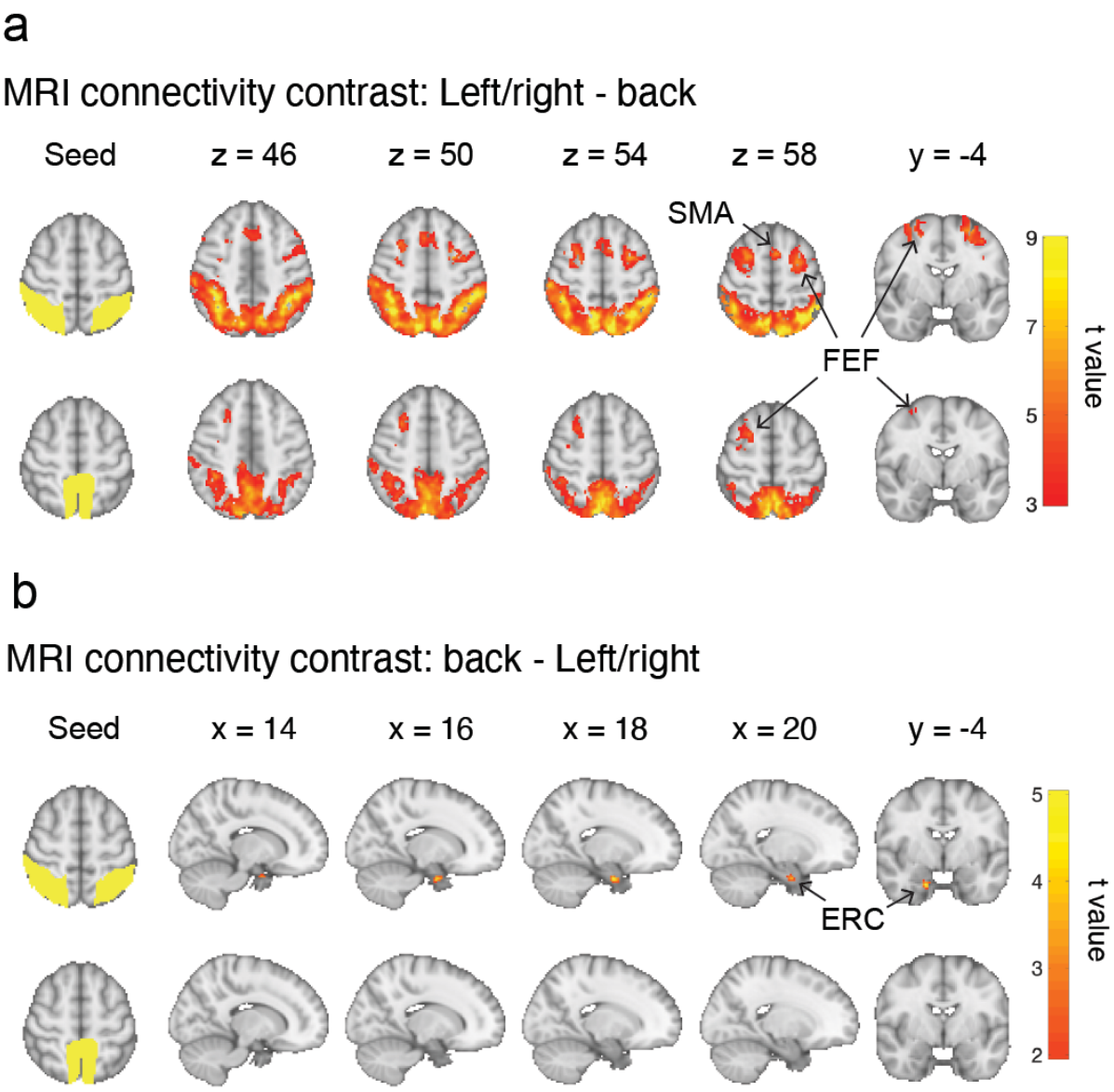


Figure 3. MRI connectivity contrast of "left/right–back" and "back–left/right" conditions using the parietal cortex and precuneus as seeds. a) For the "left/right–back," condition significant connection was found in the parietal cortex, precuneus, FEF, and SMA for both seeds ($P < 0.01$, initial threshold, $P < 0.05$, cluster-corrected for multiple comparison); b) For the "back–left/right," an increased connectivity was revealed between the parietal cortex and right ERC, which survived for small volume correction based on the mask of bilateral MTL ($P < 0.01$, initial threshold, $P < 0.05$, cluster-corrected for multiple comparison); no connection was found between precuneus and MTL regions.

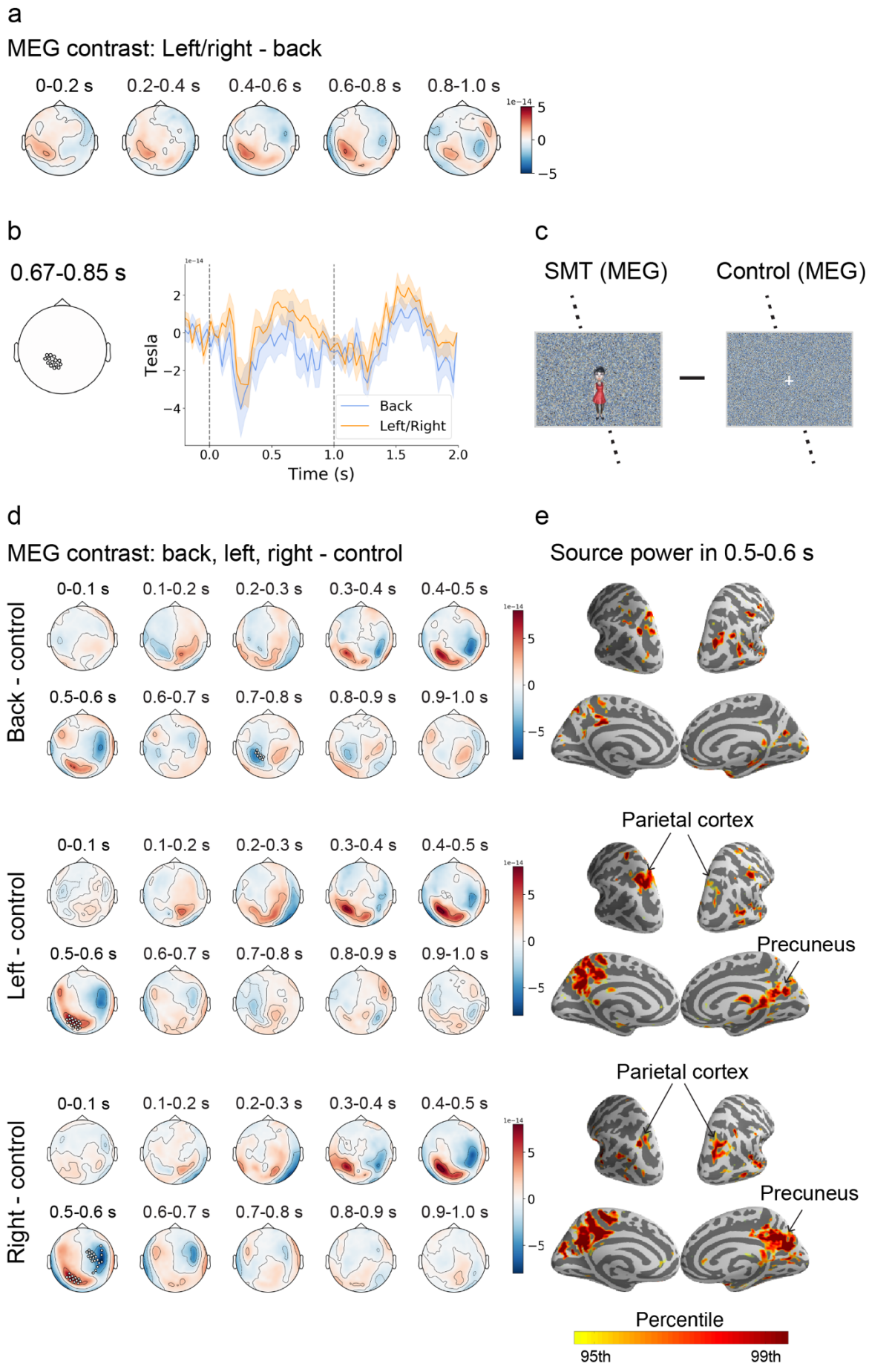


802

803 Figure 4. a) Mean topographic map for the MEG contrast of "left/right–back" condition for
804 every 0.2 s during the targeting period. b) Time courses of the signal strength on the left-
805 posterior cluster of sensors in the back-target and left/right-target conditions. A significantly
806 higher activity was found for the left/right-target condition relative to the back-target
807 condition 0.67–0.85 s after the onset of the targeting period ($P < 0.05$, initial threshold, $P <$
808 0.05, spatial-temporal cluster correction for multiple comparison, two tailed). c) A
809 comparison between the spatial-memory task (SMT) trials and the control trials in the MEG
810 experiment. d) Mean topographic map for each of the left-target, right-target, and back-target
811 conditions relative to the control condition for every 0.1 s during the targeting period.
812 Significant clusters were found in the left-posterior from 0.5 to 0.6 s for the left-target and
813 right-target conditions ($P < 0.05$, initial threshold; $P < 0.05$, cluster-corrected for multiple
814 comparison, two tailed) but not for the back-target condition. e) Source-power distribution on
815 brain surface for each of the three conditions relative to the control within 0.5–0.6 s. Color
816 bar represents percentile rank of source-power strength.
817

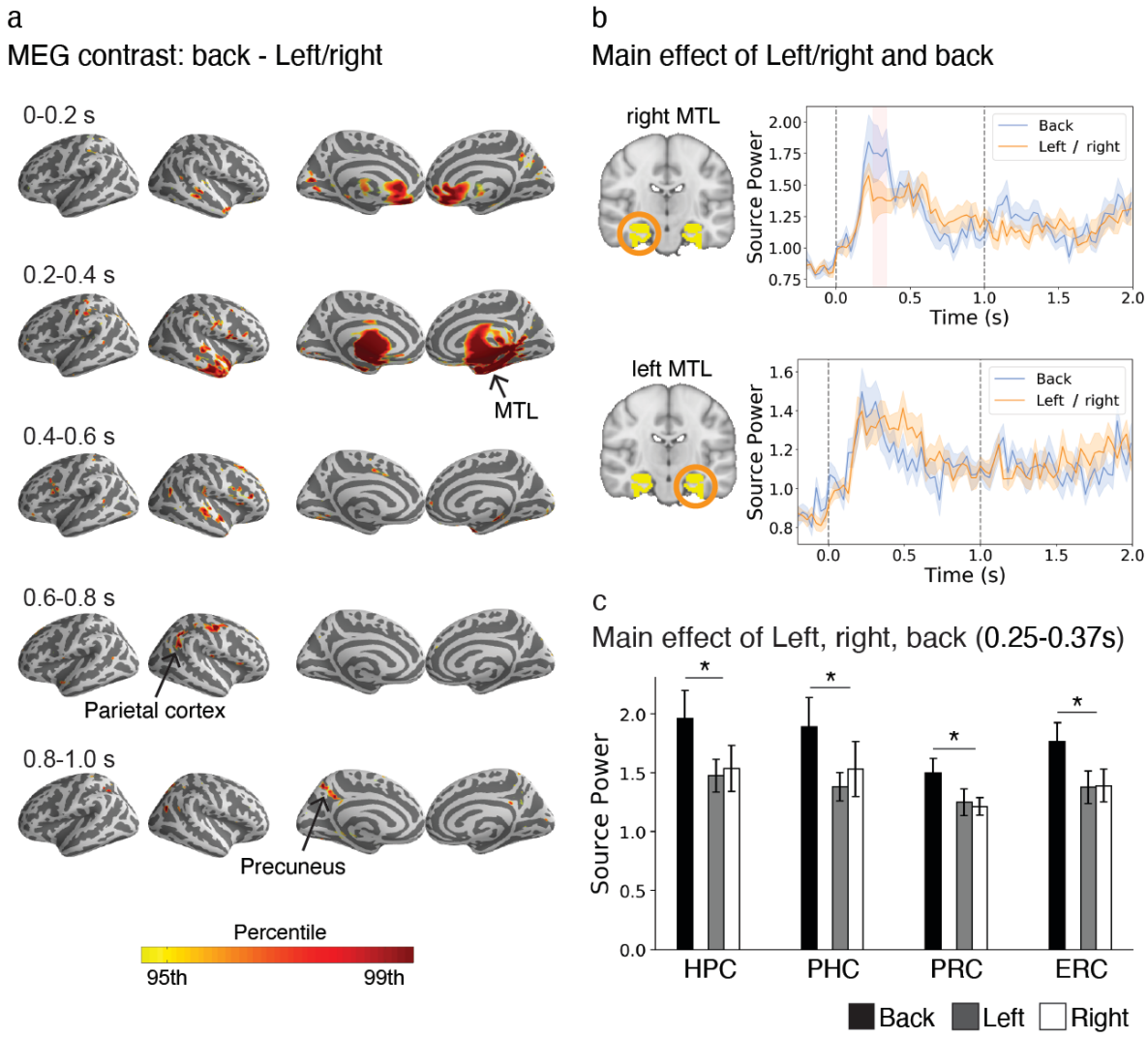


Figure 5. a) MEG contrast of "back–left/right" condition in source-power for every 0.2 s during the targeting period. Color bar represents percentile rank of source-power strength.. b) ROI analysis for both hemispheres of the MTL. Shaded area in the top panel (right MTL) show a significantly higher the source-power for the back-target condition than for the left/right-target condition 0.25–0.37 s after the onset of targeting period ($P < 0.05$, spatial-temporal cluster correction for multiple comparison, two tailed). c) ROI analysis of the source-power in each of the right MTL subregions for each condition. * $P < 0.05$, $t$ (11) = 3.00, 2.98, 3.22, and 3.39 for HPC, PHC, PRC, and ERC, respectively, two tailed, Bonferroni-corrected for multiple comparisons (n = 4). Error bar represents SEM.

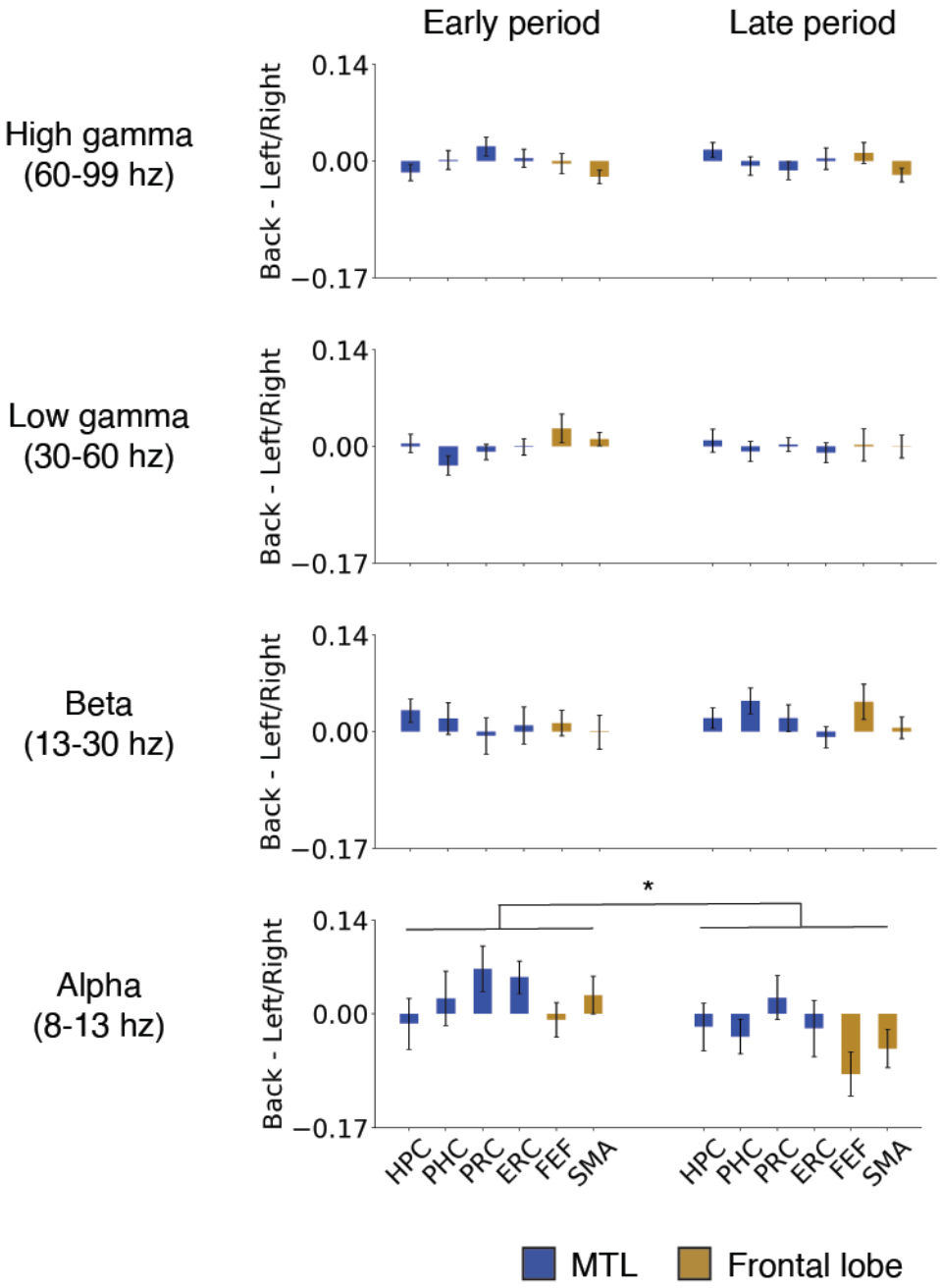


Figure 6. MEG connectivity contrast of the "back–left/right" conditions using the parietal cortex as a seed. The connectivity with each of six anatomical ROIs was estimated for alpha, beta, and gamma frequency bands using PLI during the early phase (0.08-0.48 s) and late phase (0.56-0.96 s). * $P = 0.02$, $F\,(2, 132) = 8.24$, a main effect of time-windows (early vs. late), repeated-measures two-way ANOVA with brain areas as another main effect, Bonferroni-corrected for multiple comparisons of frequency bands (n = 4).

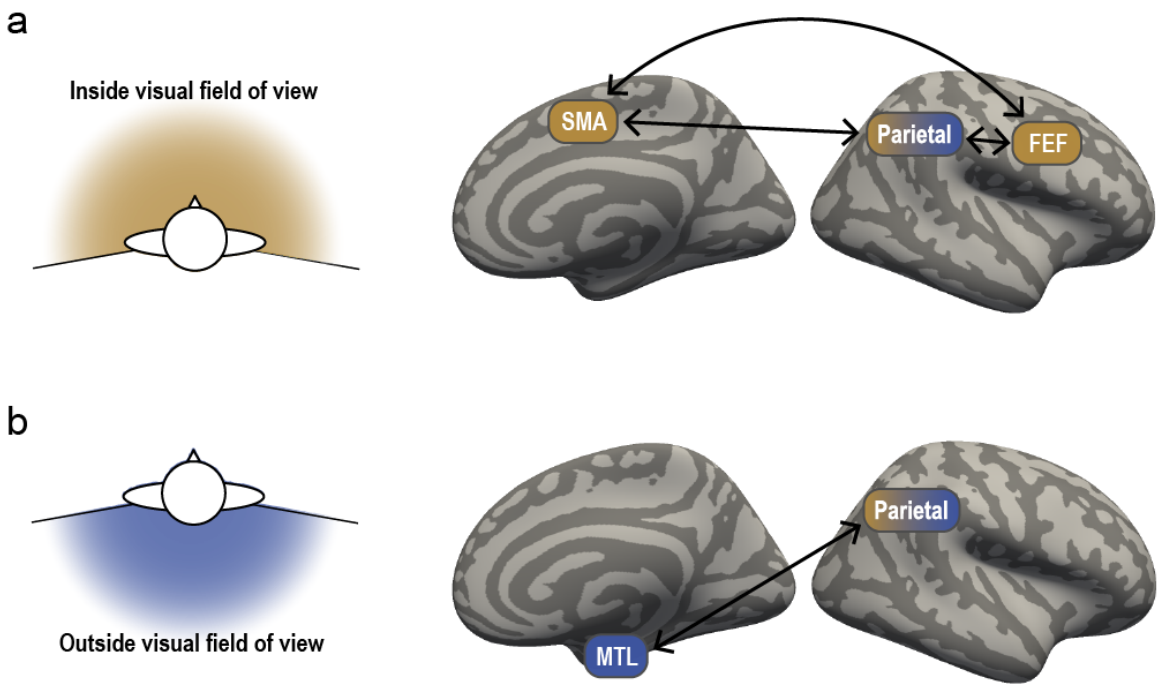


837

838 Figure 7. Two brain networks responsible for the egocentric space inside and outside of the
839 visual field. a) The fronto-parietal network represents target in the visual field (yellow shade).
840 The FEF and SMA are included in this network to represent the space in front for a
841 subsequent action. b) The MTL-parietal network represents a target outside the visual field
842 (blue shade). The right MTL, particularly ERC, is recruited in this network to represent a
843 target behind the self-body. In the present spatial memory task, the target location was
844 retrieved from the short-term memory, which a participant encoded just before retrieval
845 without a voluntary effort to memorize it.